

## Electron interferometry with nanogratings

Alexander D. Cronin and Ben McMorran

Department of Physics, University of Arizona, Tucson, Arizona 85721, USA

(Received 8 September 2006; published 26 December 2006)

We present an electron interferometer based on near-field diffraction from two nanostructure gratings. Lau fringes are observed with an imaging detector, and revivals in the fringe visibility occur as the separation between gratings is increased from 0.2 to 2.7 mm. The oscillations in visibility depend predictably on the wavelength of incident electrons. This verifies that 5 keV electrons diffracted by nanostructures remain coherent after propagating farther than the Talbot length, and hence proves that a Talbot-Lau interferometer for electrons can be built with nanostructure gratings. Distorted fringes due to a phase object are used to demonstrate an application for this type of electron interferometer.

DOI: [10.1103/PhysRevA.74.061602](https://doi.org/10.1103/PhysRevA.74.061602)

PACS number(s): 03.75.-b, 61.14.-x

Near-field interference effects that result in self-similar images of a periodic structure were noticed by Talbot in 1836, and later described as Fourier images [1–3]. One remarkable feature of these images is that revivals in visibility occur as the plane of observation is separated from the periodic structure by multiples of the distance  $d^2/\lambda$ , with  $d$  being the period of the structure and  $\lambda$  the wavelength of the light (or de Broglie waves) illuminating the structure. Twice this distance is known as the Talbot length  $z_T=2d^2/\lambda$ . At least partially coherent waves are required to observe self-images of a single grating (the Talbot effect). However, a related phenomenon (the Lau effect) occurs with incoherent light if *two* gratings are used [3–5]. Fringes are then formed behind the second grating, and the fringe visibility oscillates as a function of grating separation. These so-called Lau fringes can be observed directly on a screen, thus making a Lau interferometer as shown in Fig. 1.

Here we present a Lau interferometer for electrons based on two nanostructure gratings that each have a period of  $d=100$  nm. With medium energy (5 keV) electrons that have a de Broglie wavelength of  $\lambda=17$  pm, the Talbot length is 1.16 mm. An imaging detector 80 cm beyond the gratings was used to observe the Lau fringes shown in Fig. 2, and the fringe visibility as a function of grating separation is plotted in Fig. 3. Revivals in fringe visibility are observed to occur at exactly the half-integer multiples of the Talbot length as predicted in [3–5]. To further support the claim that these are Lau fringes, i.e., fringes due to wave interference effects, we present evidence that the fringe revival spacing changes pre-

dictably with de Broglie wavelength (also shown in Fig. 3). If the fringes are analyzed with a third grating (even a digital mask in the image processing can achieve this purpose), then this apparatus serves as a Talbot-Lau interferometer. However, even more information is gained by studying images of the Lau fringes directly.

Interferometers based on the Talbot and Lau effects have found applications in light optics [3,5,6], in atom optics [7–11], and more recently with x rays [12]. Yet even though electron interferometry is a mature field [13–16], neither Lau nor Talbot-Lau interferometer designs have been operated with electrons until now.

Perhaps the chief reason that Talbot-Lau interferometers have not previously been created for electrons is that suitable periodic structures have not been available. Crystals with a lattice period on the order of 1 nm can serve as a grating, but at typical transmission electron microscope energies the resulting Talbot length (less than 200 nm) is too short for many practical interferometer experiments [17]. A further complication is that the angular misalignment of the two gratings must be smaller than one grating period over the height of the beam. Hence alignment within  $10^{-6}$  rad would be required for a Lau interferometer built with crystal gratings and a 1-mm-high incoherent beam. These limitations are overcome by using nanostructure gratings with a 100 nm period capable of coherently transmitting electrons. Then the Talbot length is increased to 1 mm, and the alignment tolerance for a Lau interferometer is relaxed to  $10^{-3}$  rad.

Nanostructure gratings are not new. In 1959 Möllenstedt

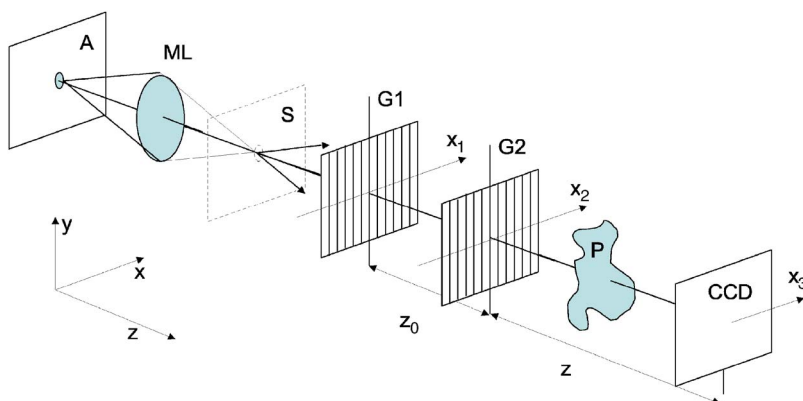


FIG. 1. (Color online) Lau interferometer for electrons. There is a variable aperture (50–200  $\mu\text{m}$ ) at plane A, a magnetic lens ML, a beam focus ( $\sim 10$   $\mu\text{m}$  beam waist) at plane S, nanogratings G1 and G2, an optional phase object at plane P, and a charge-coupled device (CCD) imaging screen. In our experiments  $z_0$  is in the range 0–3 mm, and  $z=80$  cm. The distance between S and G1 is typically 2 cm, and the divergence of the beam from S is  $5 \times 10^{-3}$  rad. Not shown: the thermionic tungsten filament, grid cap, and condenser lens are located before A.

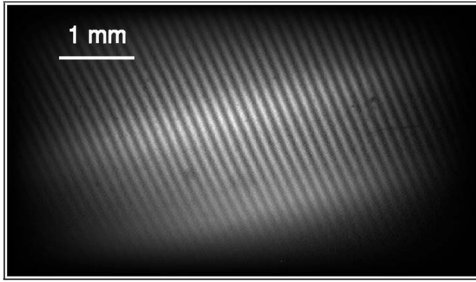


FIG. 2. Lau fringes formed with 5 keV electrons and two 100-nm-period gratings separated by 0.6 mm (half the Talbot length). This figure was obtained by imaging a phosphor screen with a CCD.

and Jönsson [18,19] were able to diffract 50 keV electrons using five slits in a copper foil spaced by  $1\ \mu\text{m}$ . Other examples of diffractive nanostructures for electron optics use surface features supported on top of a substrate [20,21], but due to the material thickness none of these transmit low-energy electrons as well as the fully perforated gratings that we use here. The gratings that we use are fabricated by Savas *et al.* [22], and were recently used to study electron diffraction [23–25]. Results presented here confirm that these gratings can be used for interferometry with medium-energy (3–5 keV) electrons.

In the rest of this paper we describe the electron optics setup, and briefly discuss the diffraction theory used to model the revivals in Fig. 3. We comment on the role of image charge interactions between electrons and the nanogratings. Then we demonstrate an application of this interferometer: the study of the index of refraction for electrons due to fields around a charged needle tip.

Lau fringes have highest visibility when the grating separation ( $z_0$ ) and the distance to the screen ( $z$ ) satisfy

$$\frac{z_0 z}{z_0 + z} = \frac{nd^2}{\lambda}. \quad (1)$$

Then the period of the Lau fringes is

$$d' = d \frac{z_0 + z}{z_0}, \quad (2)$$

where  $d$  is the period of the gratings. Equations (1) and (2) are derived in the Fresnel approximation in Refs. [3,6,11]. Because the distance to the screen is typically 800 times as long as the separation between gratings ( $z/z_0=800$ ) in our experiment, the fringes are effectively magnified so that  $d' = 800d$ . The ratio of periods for G1, G2, and the detected fringes is therefore 1:1:800.

To model the shape and visibility  $V \equiv (I_{\max} - I_{\min}) / (I_{\max} + I_{\min})$ , of the fringes as a function of grating separation we used a calculation described in reference [11] to evaluate the Fresnel-Kirchhoff integral:

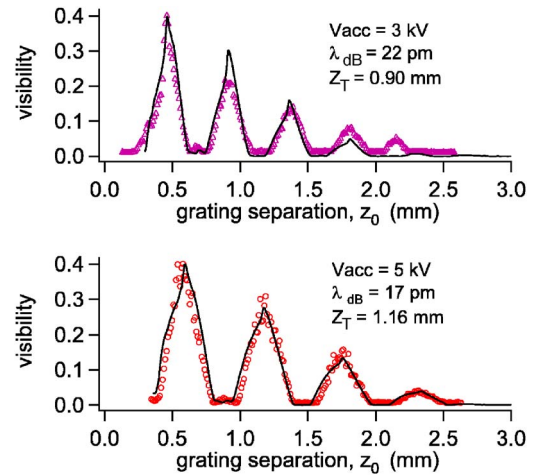


FIG. 3. (Color online) Revivals in fringe visibility as a function of grating separation ( $z_0$ ). Data (symbols) are compared to theory (line) from Ref. [11] for two gratings each with 40% open fraction. Visibility maxima are found when the gratings are separated by a half-integer number of Talbot lengths, and this depends on the electron accelerating voltage ( $V_{\text{acc}}$ ). The maximum visibility is 40% for both the 3 and 5 keV electrons (the theory curve has been scaled down to account for background signal in the experiment). Visibility decays when the fringe period is comparable to the resolution of the detector.

$$I(x_3, x_1) \propto \left| \int t_2(x_2) \exp\left(i \frac{2\pi}{\lambda} (\ell_1 + \ell_2)\right) dx_2 \right|^2 \quad (3)$$

where  $t_2$  is the amplitude transmission function of G2,  $\ell_1 = \sqrt{z_0^2 + (x_2 - x_1)^2}$ , and  $\ell_2 = \sqrt{z^2 + (x_3 - x_2)^2}$  (see Fig. 1). The function  $t_2$  is described in [23,24]. Equation (3) describes the intensity at point  $x_3$  on a screen due to waves originating from point  $x_1$  in the plane of G1. All possible paths from  $x_1$  to  $x_2$  (incurring path length  $\ell_1$ ) and subsequently from  $x_2$  to  $x_3$  (incurring path length  $\ell_2$ ) interfere at  $x_3$ . This represents coherent diffraction of waves by grating G2. Next the model allows for the width of the incident beam the finite size of the windows in the first grating by summing intensities:

$$I(x_3) = \int |t_1(x_1)|^2 I(x_3, x_1) dx_1 \quad (4)$$

where  $t_1$  is the amplitude transmission function of G1. This theory was used to generate the curves in Fig. 3 and the theoretical portion of Fig. 4.

We emphasize that the fringe visibility in this wave-optics model is insensitive to the size of the incident beam, but does depend on the wavelength as summarized by Eq. (1). Both of these features are confirmed with our data: revivals in visibility are observed to occur when the grating spacing  $z_0$  satisfies Eq. (1) regardless of the lens and aperture settings. In addition, this model predicts the fractional Talbot effect, in which fringes with half the period predicted by Eq. (1) are formed when  $z_0 = 3/4 z_T$ . These half-period revivals are also observed in the data (see Figs. 4 and 5 at G1-G2 separation of  $z_0 = 0.85$  mm).

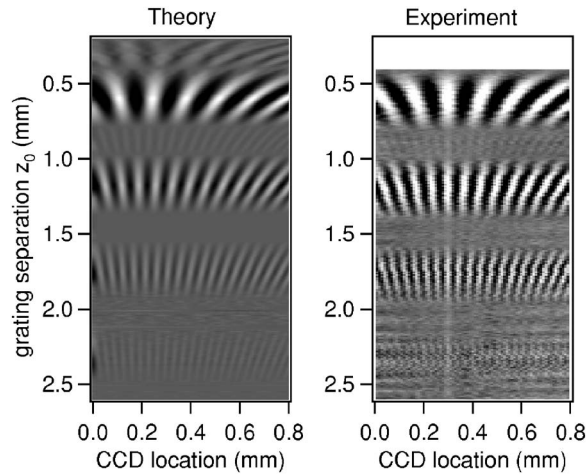


FIG. 4. Lau fringes vs grating separation for 5 keV electrons. (Theory) The theoretical composite was generated with the theory given in Ref. [11]. A point spread function for the imaging detector (Gaussian with rms  $40 \mu\text{m}$ ), and the open fraction of the gratings (40%) is included in the theory. (Experiment) Each row in this composite image is a row from a different raw image obtained with different values of G1-G2 separation ( $z_0$ ). To compensate for experimental noise in the transverse position of the gratings, which leads to phase shifts in the fringes, each row has been shifted to locate a maximum at position 0.3 mm.

While a classical ray-optics model based on the shadows of two gratings can predict magnified (projected) grating images and also revivals in visibility, we note here that a ray-optics model fails to explain several features of our data. For example, classical ray models predict that the revival spacing depends strongly on the beam width and is independent of beam wavelength. It also fails to predict the half-period revivals. Finally, the Fresnel number for our setup is  $F = d^2/\lambda z_0 \approx 1$ , and in general ray optics is valid only when the Fresnel number for a system is far greater than 1. Thus, a classical Moiré interpretation is insufficient to describe this experiment.

Our experimental data are best fit by a grating transmission function for G1 and G2 that is described by a 40% open fraction (which agrees with independent measurements), and a weak image-charge interaction between electrons and the

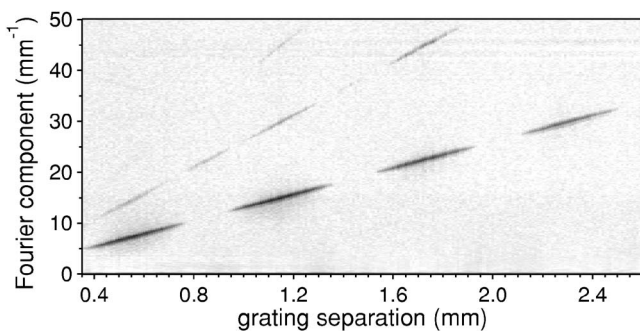


FIG. 5. Power spectra of Lau fringes vs grating separation for 5 keV electrons. Each column of pixels is generated by a Fourier transform of a row of data in Fig. 4. Note that the fractional Talbot effect produces the double-spatial-frequency features at 0.85 mm.

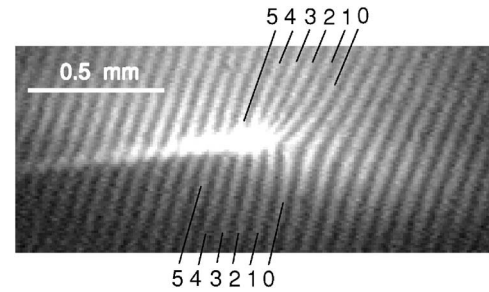


FIG. 6. Distorted fringes around the shadow of a charged needle placed in plane P (Fig. 1). Consecutive fringes are labeled on the top and bottom to emphasize the discontinuity that arises due to the wire acting as a biprism. The  $100\text{-}\mu\text{m}$ -diameter wire was held at 4.5 V, and surrounded by a grounded cylinder of radius 3 cm.

grating bars. The image-charge interaction was discussed in detail in [23,24], and it has a similar effect on the electron optics as the Casimir-Polder interaction does for atom optics [11,26,27]. We include the strength of the image charge as a free parameter in the transmission function  $t_2$  for the second grating. The best fit with the data was obtained using an image charge of  $q' = 0.03|e|$ .

Additional analysis of the shape of the fringes was accomplished by taking the Fourier transform of images such as Fig. 2. These image transforms show how the spatial frequency of the fringes change with grating separation. A composite image of fringe spectra, in which each vertical column in the image represents the one-dimensional spatial frequency spectrum of fringes for a specific grating separation ( $z_0$ ), is shown in Fig. 5. As in Fig. 4, the fractional Talbot effect is clear at the grating separation  $z_0 = 0.85$  mm. The higher harmonics of spatial frequency indicate that the fringes are not purely sinusoidal, but tend in places to look more like the binary (Ronchi rule) masks made by ideal absorbing nanostructure gratings. This is the self-imaging property of the Talbot and Lau effects.

To demonstrate that this interferometer can be used to study phase shifts for electrons due to various objects, we inserted a charged wire in the beam after the second grating in plane P of Fig. 1. Like a lightning rod, the tip of the wire causes large gradients in electric potential. The electric potential in the space around the wire changes the index of refraction for electron waves and distorts the interference fringes as shown in Fig. 6.

Multiple paths through the interferometer sample different parts of the phase object; therefore we are sensitive only to gradients in the index of refraction, not the index directly. This design is known as a shearing interferometer and shifts in fringe position are proportional to  $[\partial/\partial x]\Phi(x,y)$  and distortion in the fringes is associated with  $[\partial/\partial x]^2\Phi(x,y)$ , where  $\Phi(x,y) = \int n(x,y,z)k_0 dz$ , with  $n(x,y,z)$  being the index of refraction [3,5,6,12,15]. For electron de Broglie waves this is  $\Phi(x,y) = \int \sqrt{(2m/\hbar^2)[E + e|V(x,y,z)]} dz$  where  $V(x,y,z)$  is the electric potential,  $E$  the incident energy of the electrons,  $m$  the electron mass,  $e$  the magnitude of the electron charge, and  $\hbar$  Planck's constant divided by  $2\pi$ . Thus, this interferometer is sensitive only to gradients in potential energy, i.e., forces.

A continuous wire produces a uniform linear phase gradient  $[\nabla\Phi(x,y)]$  with opposite sign on either side of the wire. That is how it serves as a biprism [14]. Around the tip of the freely suspended charged wire, however, there is a strong double-gradient term  $[\nabla^2\Phi(x,y)]$ . Hence fringe distortion is expected around the tip of the charged wire, and uniform fringe shifts are expected along the sides. Since the shifts are perpendicular to the wire, and in general the wire can be skew to the grating bars, fringes on either side of the wire can appear out of step as indicated in Fig. 6. This serves as a proof of principle that the interferometer setup presented here can be used to study differential phase shifts due to a phase object.

We are aware of the construction of a Mach-Zehnder electron interferometer by Batelaan and co-workers, which requires a much higher degree of electron spatial coherence than our interferometer [28]. Our results are distinct in that we use an incoherent electron beam and we image electron interference fringes directly. The imaging tool allows us to detect fringes with arbitrary period ( $d'$ ), and thus permitted us to study quantitatively the revivals in fringe visibility as a function of grating separation. Imaging also enabled us to observe the fractional Talbot effect with electrons and nano-

structures. The most useful result of using an imaging detector is the ability to study fringe distortions due to phase objects in the electron interferometer.

In conclusion, we demonstrated an electron interferometer that uses two nanostructure gratings and near-field interference effects. We demonstrated the Lau effect for electrons and observed revivals in fringe visibility when the gratings are separated by multiples of the Talbot length. This type of electron interferometer does not require spatially coherent electron waves from the electron gun, but still it tests how well the nanostructures generate and preserve coherence for electron waves. The effect of image-charge interactions between electrons and the grating structure was observed, but it does not inhibit the electron interference. The apparatus is a rudimentary shearing interferometer, and serves to demonstrate differential phase shifts. We have thus shown that metal-coated silicon nitride nanostructure gratings can be used as elements for coherent electron optics.

The authors acknowledge D. Bentley for the electron gun, and Mark Robertson-Tessi for technical assistance. This work was supported by the National Science Foundation Grant No. 0354947 and No. 0526954.

- 
- [1] H. F. Talbot, *Philos. Mag.* **9**, 401 (1836).  
 [2] J. M. Cowley and A. F. Moodie, *Proc. Phys. Soc. London* **70**, 486 (1957); **70**, 497 (1957); **70**, 505 (1957); **76**, 378 (1960).  
 [3] K. Patorski, *Prog. Opt.* **27**, 3 (1989).  
 [4] E. Lau, *Ann. Phys.* **6**, 417 (1948).  
 [5] J. Jahns and A. W. Lohmann, *Opt. Commun.* **28**, 263 (1979); H. O. Bartelt and J. Jahns, *ibid.* **30**, 268 (1979).  
 [6] D. E. Silva, *Appl. Opt.* **11**, 2613 (1972).  
 [7] M. S. Chapman, C. R. Ekstrom, T. D. Hammond, J. Schmiedmayer, B. E. Tannian, S. Wehinger, and D. E. Pritchard, *Phys. Rev. A* **51**, R14 (1995).  
 [8] S. Nowak, C. Kurtsiefer, T. Pfau, and C. David, *Opt. Lett.* **22**, 1430 (1997).  
 [9] J. F. Clauser and S. Li, *Phys. Rev. A* **49**, R2213 (1994).  
 [10] B. Brezger, L. Hackermuller, S. Uttenthaler, J. Petschinka, M. Arndt, and A. Zeilinger, *Phys. Rev. Lett.* **88**, 100404 (2002).  
 [11] B. Brezger, M. Arndt, and A. Zeilinger, *J. Opt. B: Quantum Semiclassical Opt.* **5**, S82 (2003).  
 [12] C. David *et al.*, *Appl. Phys. Lett.* **81**, 3287 (2002); A. Momose *et al.*, *Jpn. J. Appl. Phys., Part 2* **42**, L866 (2003); A. Momose, *Jpn. J. Appl. Phys., Part 1* **44**, 6355 (2005); T. Weitkamp *et al.*, *Appl. Phys. Lett.* **86**, 054101 (2005).  
 [13] L. Marton, *Phys. Rev.* **85**, 1057 (1952); L. Marton, S. J. A., and H. A. Suddeth, *Rev. Sci. Instrum.* **25**, 1099 (1954).  
 [14] G. Möllenstedt and H. Düker, *Z. Phys.* **145**, 377 (1956).  
 [15] A. Tonomura, *Rev. Mod. Phys.* **59**, 639 (1987); *Electron Holography* (Springer, Berlin, 1999).  
 [16] E. Völkl, L. Allard, and D. Joy, *Introduction to Electron Holography* (Kluwer Academic/Plenum Press, New York, 1999).  
 [17] For this calculation we assumed 100 keV electrons with a de Broglie wavelength of  $\lambda=3.9$  pm. Lower-energy electrons make the Talbot length even shorter.  
 [18] G. Möllenstedt and C. Jönsson, *Z. Phys.* **155**, 472 (1959).  
 [19] C. Jönsson, *Z. Phys.* **161**, 454 (1961).  
 [20] P. Holl, *Optik (Stuttgart)* **28**, 421 (1969).  
 [21] Y. Ito, A. L. Bleloch, J. H. Paterson, and L. M. Brown, *Ultramicroscopy* **52**, 347 (1993); Y. Ito, A. L. Bleloch, and L. M. Brown, *Nature (London)* **394**, 49 (1998).  
 [22] T. A. Savas, S. N. Shah, M. L. Schattenburg, J. M. Carter, and H. I. Smith, *J. Vac. Sci. Technol. B*, **13**, 2732 (1995).  
 [23] G. Gronniger, B. Barwick, H. Batelaan, T. Savas, D. Pritchard, and A. Cronin, *Appl. Phys. Lett.* **87**, 124104(2005).  
 [24] B. McMorran, J. D. Perreault, T. A. Savas, and A. Cronin, *Ultramicroscopy* **106**, 356 (2006).  
 [25] B. Barwick, G. Gronniger, L. Yuan, S. H. Liou, and H. Batelaan, *J. Appl. Phys.* **100**, 074322 (2006).  
 [26] R. E. Grisenti, W. Schollkopf, J. P. Toennies, C. C. Hergerfeldt, and T. Kohler, *Phys. Rev. Lett.* **83**, 1755 (1999).  
 [27] J. D. Perreault, A. D. Cronin, and T. A. Savas, *Phys. Rev. A* **71**, 053612 (2005).  
 [28] G. Gronniger, B. Barwick, and H. Batelaan, *New J. Phys.* **8**, 224 (2006).